ISSN 2394-3777 (Print)
ISSN 2394-3785 (Online)
Available online at www.ijartet.com
International Journal of Advanced Research Trends in Engineering and Technology (IJARTET)
Vol. 4, Issue 4, April 2017

SUPPRESSION OF DOUBLE-FREQUENCY RIPPLE WITH ANN CONTROL FOR A SINGLE-PHASE PV QUASI-Z-SOURCE INVERTER

[1]G.POORNA, [2]T.VINAY KUMAR
[1]Assistant Professor, EEE department,Bhoj Reddy Engineering College for Women.
[2]Assistant Professor,EEE department,Bhoj Reddy Engineering College for Women.

Abstract-In this paper we are implementing a single phase photovoltaic system (PV), which have been exist a double frequency mismatch and it also exist in between the dc input side and ac output side. Therefore, according to the capacitance reduction control strategy which is proposed to buffer the DFR energy in single-phase Z-source/quasi-Z-source inverter applications. We are using the ANN control ANN is nonlinear model that is easy to use and understand compared to statistical methods. ANN is non-parametric model while most of statistical methods are parametric model that need higher background of statistic.According to the single-stage photovoltaic(PV) system, power irregularity will be existing between the AC yield and DC input.therefore the double-frequency ripple (DFR) energy will required to be buffered by passive network. In a conventional PV system, due to their high capacitance electrolytic capacitors are usually used. Electrolytic capacitors are considered to be one of the most failure prone components in a PV inverter. The proposed control strategy can significantly reduce the capacitance requirement and achieve low input voltage DFR. Consequently, highly reliable film capacitors can be used. Due to the proposed control strategy the increased switching device voltage stress and power loss will also be discussed. By using the simulation results we can analyze the proposed method.

Index Terms—Capacitance reduction, double-frequency ripple(DFR), Z-source (ZS)/quasi-Z-source (QZS), ANN control.

INTRODUCTION

In the recent years for the photovoltaic application the voltage fed z-source inverter and quasi z-source inverter are considered. This inverter features single stage buck boost transformer. It is due to shoot through capability. For the single phase and three phase applications the z-source inverter and quasi z source inverter are utilized. The voltage-fed z-source inverter (ZSI) and quasi-Z-source inverter (QZSI) has been considered for photovoltaic (PV) application in recent years [1-3]. These inverters feature single-stage buck-boost and improved reliability due to the shoot-through capability. The ZSI and QZSI are both utilized in three-phase and single-phase applications [1-5]. The singlephase ZSI/QZSI can also be connected in cascaded structure for higher voltage application and higher performance [6].

The mismatched ac ripple is termed as double-frequency ripple (DFR) in this paper. In three-phase applications, the Z-source (ZS)/ quasi-Z-source (QZS) network only needs to be designed to handle the highfrequency ripples. However, in single-phase application, the ZS/QZS network needs to handle not only the high-frequency ripples but also the low-frequency ripple. The QZSI will be used in this paper to study the low-frequency ripple issue and present the proposed control strategy. A single-phase QZSI system is shown in Fig. 1.

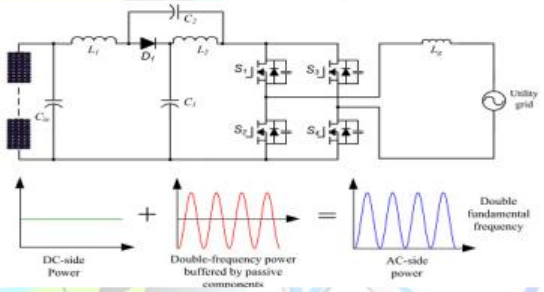

Fig. 1. Diagram of a single-phase QZSI based PV system.

Ideally, the dc-side output power is pure dc and the ac-side power contains a dc component plus ac ripple component whose frequency is two times the grid voltage frequency. The mismatched ac ripple is termed as double-frequency ripple (DFR) in this paper. In order to study the low frequency ripple issues QZSI is used in this paper. A single phase QZSI system is shown in fig.1. The output power at DC side is pure DC and AC side power contains DC component plus AC ripple component whose frequency is two times the grid frequency. The mismatched AC ripple in the system is coined as double frequency ripple (DFR).

In this paper, a new control strategy is proposed for ZSI/ QZSI to mitigate the input DFR without using large capacitance, which enables us to use the highly reliable film capacitors. There is no

ISSN 2394-3777 (Print)
ISSN 2394-3785 (Online)
Available online at www.ijartet.com
International Journal of Advanced Research Trends in Engineering and Technology (IJARTET)
Vol. 4, Issue 4, April 2017

extra hardware needed to implement the capacitance reduction. The proposed control system incorporates a modified modulation strategy and a DFR suppression controller. The gallium nitride (GaN) devices are applied in the inverter to increase the system efficiency at high switching frequency. Finally, experimental results are provided to verify the effectiveness of the proposed control system.

In order to balance the power mismatch between the dc side and ac side, the DFR power needs to be buffered by the passive components, mainly the QZS capacitor C_1 which has higher voltage rating than C_2. The DFR peak power is the same as the dc input power, so large capacitance is needed to buffer this ripple energy. To achieve high inverter power density with reasonable cost, electrolytic capacitors are usually selected. Christo Ananth et al.[5] presented a brief outline on Electronic Devices and Circuits which forms the basis of the Clampers and Diodes.

Two additional smoothing-power circuits are employed to reduce the DFR of DC-link voltage in ZSI. However, the added circuits increase the system cost and complexity. A low-frequency harmonic elimination PWM technique is presented to minimize the doublefrequency ripple on Z-source capacitors. However, the method is used for application with constant voltage input source and double-frequency ripple current is induced in the inductor and the input side. This is not suitable for the PV application, because the ripple current will decrease the energy harvest from the PV panels.

PROPOSED CONTROL SYSTEM FOR CAPACITANCE REDUCATION

The basic principle of the proposed capacitance reduction method can be explained by (1).

$$\Delta E = \frac{1}{2} C (v_{C-max}^2 - v_{C-min}^2) \quad (1)$$

Where C is the capacitance, ΔE is the ripple energy that is stored in the capacitor, and $V_{C\text{-}max}$ and $V_{C\text{-}min}$ are the maximum and minimum voltages across the capacitor. According to (1), there are two ways to increase ΔE. One is to increase the capacitance C, and the other way is to increase the voltage fluctuation across the capacitor. Instead of increasing the capacitance, the proposed control system will increase the voltage fluctuation across the QZS capacitors to buffer more double-frequency power. A dedicated strategy is needed to impose the DFR on QZS capacitors while preventing the ripple energy from flowing into the input.

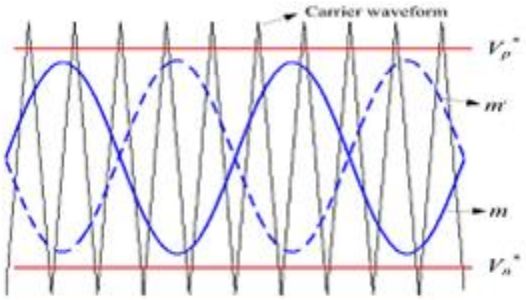

(a)

Fig. 2. The modulation strategy of (a) traditional method

In conventional single-phase QZSI, the modulation strategy is shown in Fig. 2(a). The two-phase legs of the full bridge are modulated with 180o opposed reference waveforms, m and, m^1 to generate three-level voltage output. Two straight lines V_p^* and V_n^* are used to generate the shoot through duty ratio. When the triangular carrier is greater than v*p or the carrier is smaller than V_n^*, all four switches S1 – S4 turn on simultaneously for shoot-through.

In the proposed control system, the shoot-through control lines V_p^* and V_n^* are modified to a line with double frequency component as shown in Fig. 2(b).

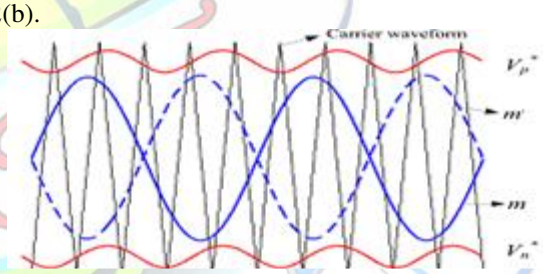

(b)

Fig. 2. The modulation strategy of (b) proposed method.

By doing so, the dc side and the QZS capacitor DFR can be decoupled. An input DFR suppression controller is added in the control system to generate the double-frequency component in V_p^* and V_n^*.

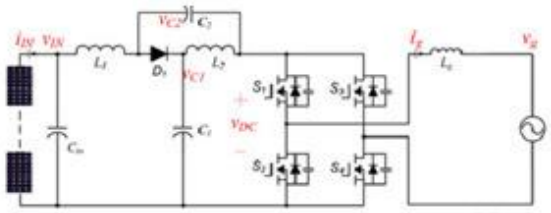

ISSN 2394-3777 (Print)
ISSN 2394-3785 (Online)
Available online at www.ijartet.com
International Journal of Advanced Research Trends in Engineering and Technology (IJARTET)
Vol. 4, Issue 4, April 2017

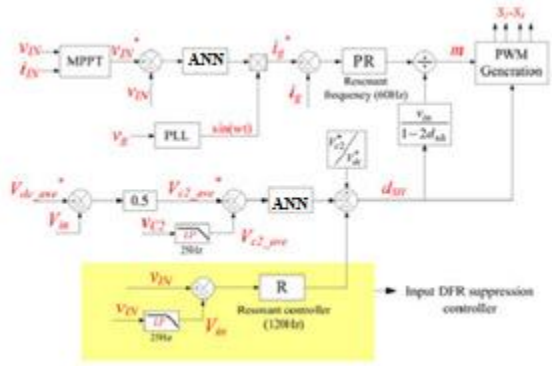

Fig. 3. Diagram of the proposed control system.

Fig. 3 shows the detailed control system diagram of the proposed single-phase QZSI. The proposed control contains the maximum power point tracking (MPPT) controller, grid connected current controller, QZS capacitor voltage controller and input DFR suppression controller. The MPPT controller provides the input voltage reference V_{IN}^*. The error between V_{IN}^* and$V_{IN}^*$is regulated by ANN controller and its output is the magnitude of the grid current reference. The grid current I_g is regulated by controlling the inverter modulation index m through a proportional resonant (PR) controller. The PR controller has a resonance frequency equal to the grid frequency. The QZS capacitor voltage is regulated bycontrolling D_{SH}. If the inverter loss is not enough to damp the oscillation, dedicated active damping is needed to deal with the oscillation and V_{C2} information is required for the implementation. Due to the limited space, the detail of the active damping is not presented in this paper and will be covered in future paper. The V_{C2} voltage controller only regulates the average value of V_{C2}, which is V_{c2_ave}, due to the low-pass filter in the signal feedback with a cutoff frequency of 25Hz. Therefore, the capacitor voltage controller has limited influence on doublefrequency component and most DFR energy can be kept in QZS capacitors. $V_{dc_ave}^*$should be selected carefully so that the value of D_{SH} does not become negative because of the double-frequency swing, and the summation of D_{SH} and m is always smaller than 1. A feedforward component V_{c2}^*/ $V_{dc\_ave}^*$ is added to the output of the capacitor voltage controller to increase the dynamic performance.

IMPACT OF CAPACTICANCE REDUCTION

A. System stability

In order to apply the proposed control system, it is necessary to study impact of decreasing C1 on system stability. The possible operation states of voltage fed QZSI have been presented in and it is summarized in the appendix with equivalent circuits, and the averaged model of QZSI can be obtained as in (2).

$$\begin{cases} L_1\frac{di_{L1}}{dt} = \left(1+\frac{T_{AB}+T_{0B}}{T_s-T_{AB}-T_{0B}}\right)(v_{C1}+v_{C2})d_{SH} + \frac{T_{SBU}}{T_s-T_{AB}-T_{0B}}(v_{C1}+v_{C2}) - v_{C1} + v_{1N} \\ L_2\frac{di_{L2}}{dt} = \left(1+\frac{T_{AB}+T_{0B}}{T_s-T_{AB}-T_{0B}}\right)(v_{C1}+v_{C2})d_{SH} + \frac{T_{SBU}}{T_s-T_{AB}-T_{0B}}(v_{C1}+v_{C2}) - v_{C2} \\ C_1\frac{dv_{C1}}{dt} = i_{L1} - (i_{L1}+i_{L2})d_{SH} - \frac{T_{SBU}}{T_s}(i_{L1}+i_{L2}) - \left(\frac{T_{AC}}{T_s}+\frac{T_{AB}}{T_s}\right)i_{DC} \\ C_2\frac{dv_{C2}}{dt} = i_{L2} - (i_{L1}+i_{L2})d_{SH} - \frac{T_{SBU}}{T_s}(i_{L1}+i_{L2}) - \left(\frac{T_{AC}}{T_s}+\frac{T_{AB}}{T_s}\right)i_{DC} \end{cases} \quad (2)$$

where T s is the switching period, T_{AB}, T_{0B}, T_{SBU}, T_{AC}, and T_{SBI} are time intervals of different operation states, as listed in the appendix, m is the modulation signal and $D_{SH} = T_{SBI} / T_s$. The small signal model can be derived accordingly as in (3).

$$\begin{cases} L_1\frac{d\hat{\imath}_{L1}}{dt} = \left(1+\frac{T_{AB}+T_{0B}}{T_s-T_{AB}-T_{0B}}\right)(v_{C1}+v_{C2})\hat{d}_{SH} + \frac{T_{SBU}}{T_s-T_{AB}-T_{0B}}(\hat{v}_{C1}+\hat{v}_{C2}) - (1-D_{sh})\hat{v}_{C1} + D_{sh}\hat{v}_{C2} + v_{1N} \\ L_2\frac{di_{L2}}{dt} = \left(1+\frac{T_{AB}+T_{0B}}{T_s-T_{AB}-T_{0B}}\right)(v_{C1}+v_{C2})d_{SH} + \frac{T_{SBU}+T_{AB}+T_{0B}}{T_s-T_{AB}-T_{0B}}(\hat{v}_{C1}+\hat{v}_{C2}) - (1-D_{sh})\hat{v}_{C2} + D_{sh}\hat{v}_{C1} \\ C_1\frac{d\hat{v}_{C1}}{dt} = \left(1-D_{Sh}-\frac{T_{SBU}}{T_s}\right)\hat{\imath}_{L1} - \left(D_{Sh}+\frac{T_{SBU}}{T_s}\right)\hat{\imath}_{L2} + (I_{l1}+I_{l2})\hat{d}_{SH} - \left(\frac{T_{AC}}{T_s}+\frac{T_{AB}}{T_s}\right)\hat{\imath}_{DC} \\ C_1\frac{d\hat{v}_{C1}}{dt} = \left(1-D_{Sh}-\frac{T_{SBU}}{T_s}\right)\hat{\imath}_{L1} - \left(D_{Sh}+\frac{T_{SBU}}{T_s}\right)\hat{\imath}_{L2} + (I_{l1}+I_{l2})\hat{d}_{SH} - \left(\frac{T_{AC}}{T_s}+\frac{T_{AB}}{T_s}\right)\hat{\imath}_{DC} \end{cases} \quad (3)$$

This RHP zero will limit the system dynamic response. However, the decrease of C1 will not significantly change the position of the RHP zero. There are two pairs of conjugated poles located on the imaginary axis, which indicate possible resonances at two different frequencies. The lower-frequency resonance is more related to C_1 and the higher-frequency resonance is mainly determined by C_2.

ISSN 2394-3777 (Print)
ISSN 2394-3785 (Online)
Available online at www.ijartet.com
International Journal of Advanced Research Trends in Engineering and Technology (IJARTET)
Vol. 4, Issue 4, April 2017

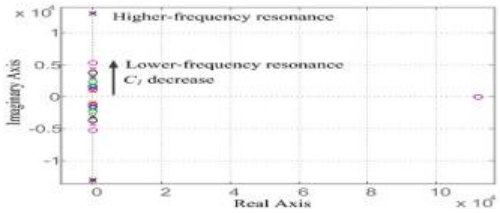

Fig. 4. Root loci of the system with C1 parameter sweeping.

Therefore, it is seen that the higher resonant frequency does not change much with the C_1 change. The lower resonant frequency increases when C1 decreases. Because there is always a zero close to the lower-frequency pole, the lower-frequency resonance is largely damped. Decreasing C1 does not affect the system stability much.

B. Increased device voltage stress and power loss

When the proposed method is applied, the double frequency voltage ripple across V_{C1} and V_{C2} will be increased intentionally. The dc link voltage across the H-bridge V_{DC} will also include DFR which could increase the voltage stress of switching devices. Because V_{C1} is much higher than V_{C2}, most double-frequency energy is stored in C1. The value of V_{C1} can be calculated using the following equation

$$\frac{1}{2}C_1 v_{C1}^2 = \frac{1}{2}C_1 v_{C1-ave}^2 + \int_0^t (P_{in} - P_{AC})dt \quad (4)$$

where $V_{c1\text{-}ave}$ is the average value of V_{C1}, P_{in} is the input power and P_{AC} is the instantaneous ac output power. P_{AC} can be calculated in (6).

$$PAC = V_{g-p}\sin(\omega t) * I_{g-p}\sin(\omega t) = \frac{1}{2}V_{g-p}I_{g-p}[1 - cos(2\omega t)] = P_{in}[1 - cos(2\omega t)] \quad (5)$$

where $V_{g\text{-}p}$ and $I_{g\text{-}p}$are the peak value of vg and I_g. Therefore, we can get

$$v_{C1} = v_{C1-ave} + \Delta v_{C1-dfr} = \sqrt{V_{c1-ave}^2 + \frac{Pin}{\omega C_1}\sin(2\omega t)} = \sqrt{\left(\frac{V_{dc-ave}+V_{in}}{2}\right)^2 + \frac{Pin}{\omega C_1}\sin(2\omega t)} \quad (6)$$

where Δvc _1 dfr is the DFR component of vC1. In (7), the value of Vin and Pin are determined by the PV array operating point. V_{dc_ave} is indirectly controlled by regulating Vc2_ave as shown in Fig.3. Therefore, when V_{dc_ave*} is selected and the PV array operating point is determined, V_{C1} can be calculated. It is seen that larger $\Delta V_{c1\text{-}dfr}$can reduce the size of C1. V_{DC} during non-shoot period can be obtained as

$$v_{DC} = 2v_{C1} - v_{in} = 2\sqrt{\left(\frac{V_{dc-ave}+V_{in}}{2}\right)^2 + \frac{P_{in}}{\omega C_1}\sin(2\omega t)} - V_{in} \quad (7)$$

It is seen from (8), when C1 and Pin are fixed, the switching device voltage stress is mainly determined by V_{dc_ave} and V_{in}. There is an optimized value of V_{dc_ave*} for different input voltage conditions to minimize the switching device voltage stress.

$$m = \frac{V_{g-p}\sin(\omega t)}{v_{DC}} \quad (8)$$

In order to take advantage of the buck-boost feature of the QZSI, the input voltage range is usually selected that Vg-p is among the input voltage range. For the proposed method, the maximum switching device voltage stress could happen at maximum or minimum Vin. When Vin is larger than Vg-p, no shoot-through is needed in conventional design and D_{SH} equal to zero. However, for the proposed method, certain value of D_{sh_ave} is needed to make sure D_{SH} does not become negative values because of the double-frequency swing. Higher Vin leads to higher peak value of V_{DC}.

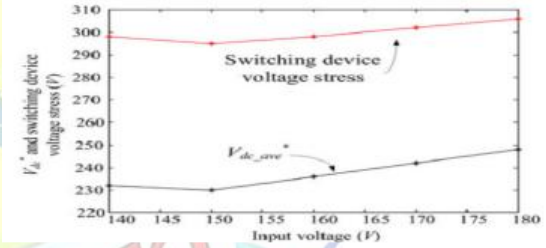

Fig. 5. V∗dc-aveand switching device voltage stress at different input voltages.

ARTIFICIAL NEURAL NETWORK

Introduction

In the last few decades, as the chemists have get accustomed to the use of computers and consequently to the implementation of different complex statistical methods. With the increasing accuracy and precision of analytical measuring methods it become clear that all effects that are of interest cannot be described by simple uni-variate and even not by the linear multivariate correlations precise, a set of methods, that have recently found very intensive use among chemists are the artificial neural networks (or ANNs for short).

Therefore, the analytical chemists are always eager to try all new methods that are available to solve such problems. One of the methods, or to say more Due to the fact that this is not one, but several different methods featuring a wide variety of different architectures learning strategies and applications.

ISSN 2394-3777 (Print)
ISSN 2394-3785 (Online)
Available online at www.ijartet.com
International Journal of Advanced Research Trends in Engineering and Technology (IJARTET)
Vol. 4, Issue 4, April 2017

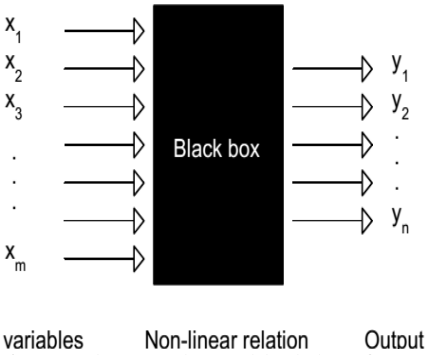

Fig 6. Neural network as a black-box featuring the non-linear relationship between the multivariate input variables and multi-variate responses

BASIC CONCEPTS OF ANNS

Artificial neuron is supposed to mimic the action of a biological neuron, i.e., to accept many different signals, xi, from many neighboring neurons and to process them in a pre-defined simple way. Depending on the outcome of this processing, the neuron j decides either to fire an output signal yj or not. The output signal (if it is triggered) can be either 0 or 1, or can have any real value between 0 and 1 (Fig. 2) depending on whether we are dealing with 'binary' or with 'real valued' artificial neurons, respectively.

The first function is a linear combination of the input variables, x1 , x2, ... xi, ... xm, multiplied with the coefficients, wji, called 'weights', while the second function serves as a 'transfer function' because it 'transfers' the signal(s) through the neuron's axon to the other neurons' dendrites. Here, we shall show now how the output, yj, on the j-th neuron is calculated. First, the net input is calculated according to equation

$$Net_j = \sum_{i=1}^{m} w_{ji} x_i \qquad (9)$$

$$y_j = out_j = 1 \Big/ \{1 + exp[-\alpha_j (Net_j + \theta_j)]\} \qquad (10)$$

The weights wji in the artificial neurons are the analogues to the real neural synapse strengths between the axons firing the signals.

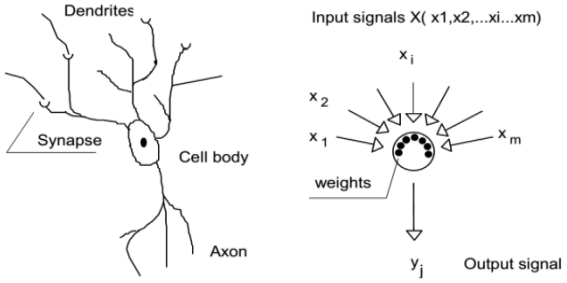

Figure 7. Comparison between the biological and artificial neuron. The circle mimicking the neuron's cell body represents simple mathematical procedure that makes one output signal yj from the set input signals represented by the multi-variate vector X.

It is important to understand that the form of the transfer function, once it is chosen, is used for all neurons in the network, regardless of where they are placed or how they are connected with other neurons. What changes during the learning or training is not the function, but the weights and the function parameters that control the position of the threshold value, qj , and the slope of the transfer function

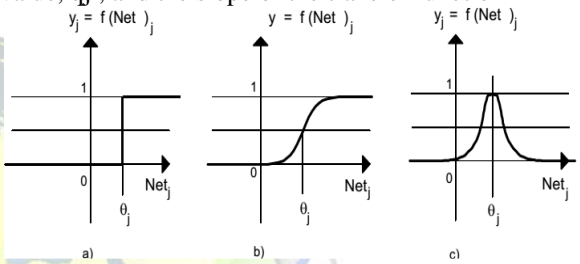

Figure 8. Three different transfer functions: a threshold (a), a sigmoidal (b) and a radial function (c). The parameter qj in all three functions decides the Netj value around which the neuron is most selective.

Therefore, Figure shows a 2-layer and a 3-layer networks with the input layer being inactive. The reader should be careful when reading the literature on ANNs because authors sometimes actually refer to the above ANNs as to the twoand three-layer ones. We shall regard only the active layer of neurons as actual layer and will therefore name this network as one and two-layer ANNs.

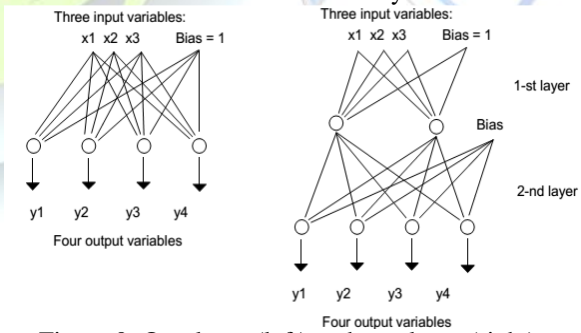

Figure 9. One-layer (left) and two-layer (right) ANNs. The ANNs shown can be applied to solve a 3-variable input 4-responses output problem

ISSN 2394-3777 (Print)
ISSN 2394-3785 (Online)
Available online at www.ijartet.com
International Journal of Advanced Research Trends in Engineering and Technology (IJARTET)
Vol. 4, Issue 4, April 2017

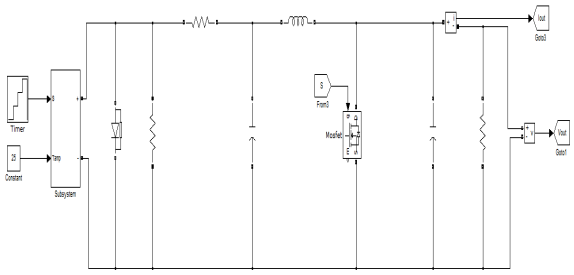

Fig.10.Block diagram of simulation

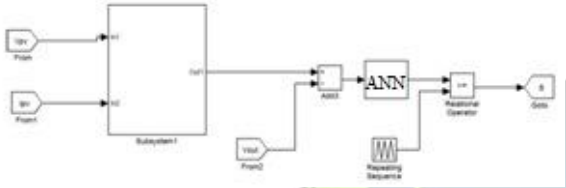

Fig.11.Control block diagram of simulation

SIMULATION RESULTS

For the proposed method, there is a design trade-off between the demand of decreasing C1 and the increased voltage stress across the switching devices.

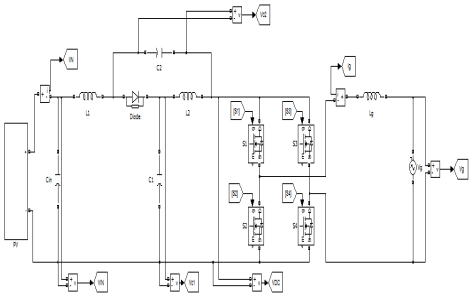

Fig.12 Block diagram of simulation

TABLE II.
PARAMETERS OF THE QZSI UNDER STUDY

qZSI Component	Parameters
Input voltage v_{IN}	140-180V
Grid voltage v_g	120Vrms
C_1	2mF for conventional system 200μF for proposed system
C_2	20μF
L_1	330μH
L_2	215μH
L_g	600μH
Switching frequency	100kHz

They are provided in Fig. 13. It is seen that the maximum voltage stress across the switching devices happens at Vin=180V in this design.

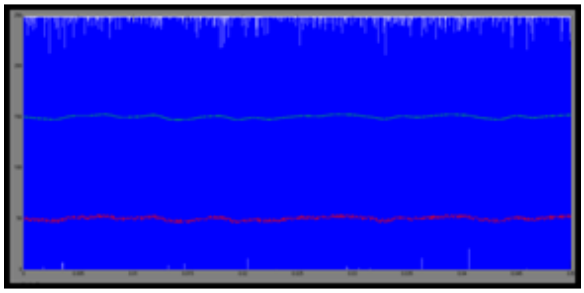

Fig. 13. The vDC, vIN and vC2 waveforms of the QZSI with the conventional control, C1=2mF.

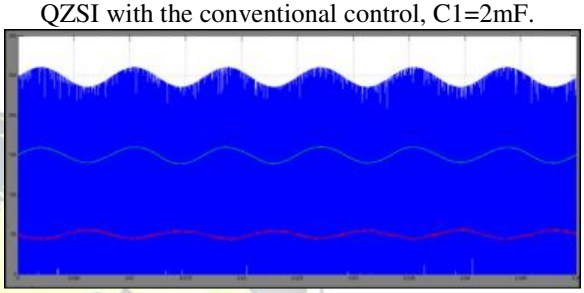

Fig. 14. The vDC, vIN and vC2 waveforms of the QZSI with the conventional control, C1=200µF

The waveforms for the QZSI with 200µF capacitor, but without the proposed control provided in Fig. 14.The waveforms of the system with the proposed control strategy are shown in Fig. 15

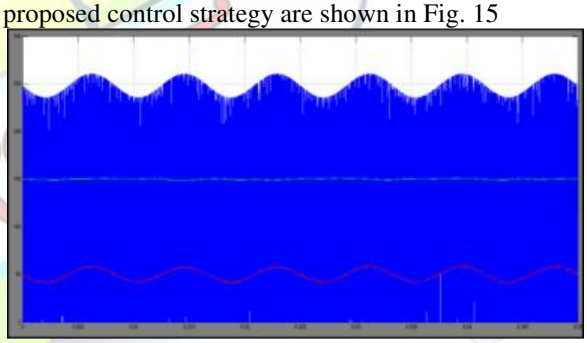

Fig. 15. The vDC, vIN and vC2 waveforms of the QZSI with the proposed control, C1=200µF.

The efficiency comparison of the conventional QZSI and the QZSI with proposed control at different power outputs is provided in Table. III.

ISSN 2394-3777 (Print)
ISSN 2394-3785 (Online)
Available online at www.ijartet.com
International Journal of Advanced Research Trends in Engineering and Technology (IJARTET)
Vol. 4, Issue 4, April 2017

TABLE III.
EFFICIENCY COMPARISON OF THE CONVENTIONAL QZSI AND QZSI WITH THE PROPOSED CONTROL

	300W	400W	500W	600W
C_1=2mF with conventional control	93.05%	93.18%	93.66%	93.76%
C_1=200μF with proposed control	92.36%	93.06%	93.48%	93.55%

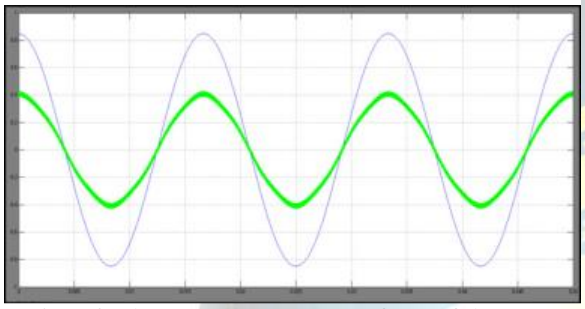

Fig. 16. The output current waveform of the QZSI with the proposed control, C1=200μF.

CONCLUSION

In this paper we are developed the newcontrol strategy which is proposed to minimize the capacitance requirement in single-phase QZSI PV system. According to the proposed control system incorporates a modified modulation strategy and a DFR suppression controller. Neural networks offer a number of advantages, including requiring less formal statistical training, ability to implicitly detect complex nonlinear relationships between dependent and independent variables, ability to detect all possible interactions between predictor variables, and the availability of multiple training algorithmsalong with another controller because of the better performance. Therefore by using large capacitance, the QZS capacitors are imposed with higher double-frequency voltages to store the double-frequency ripple energy. In ANN is non-parametric model while most of statistical methods are parametric model that need higher background of statisticbasic control action and improve the efficiency**.** Therefore in order to enhance the ripple energy flowing into the input PV side, a modified modulation and an input DFR suppression controller are used to decouple the input voltage ripple from the QZS capacitor DFR. In this paper capacitance reduction control strategy is proposed to buffer the DFR energy in Z source or Quasi Z source inverter application. The proposed control strategy can significantly reduced the capacitance requirement without using any extra hardware component. This can also achieve low input voltage DFR. Consequently,highly reliable film capacitors can used.

REFERENCES

[1] Y. Li, S. Jiang, J.G. Cintron-Rivera, and F. Z. Peng, “Modeling and Control of Quasi-Z-Source Inverter for Distributed Generation Applications,” IEEE Trans. Ind. Electron., vol.60, no.4, pp. 1532-1541, Apr. 2013.

[2] Y. Huang, M. Shen, F.Z. Peng, and J. Wang, “Z -Source Inverter for Residential Photovoltaic Systems,” IEEE Trans. Power Electron., vol.21, no.6, pp. 1776-1782, Nov. 2006.

[3] D. Cao, S. Jiang, X. Yu, and F. Z. Peng, “Low-Cost Semi-Z-source Inverter for Single-Phase Photovoltaic Systems,” IEEE Trans. Power Electron., vol.26, no.12, pp.3514-3523, Dec. 2011. [4] W. Wei, H. Liu, J. Zhang and D. Xu, “Analysis of power losses in Zsource PV grid-connected inverter,” in Proc. IEEE 8th International Conference on Power Electronics and ECCE Asia (ICPE & ECCE), May 30-Jun. 3, 2011, pp. 2588-2592.

[5] Christo Ananth, W.Stalin Jacob, P.Jenifer Darling Rosita. "A Brief Outline On ELECTRONIC DEVICES & CIRCUITS.”, ACES Publishers, Tirunelveli, India, ISBN: 978-81-910-747-7-2, Volume 3,April 2016, pp:1-300.

[6] L. Liu, H. Li, Y. Zhao, X. He, and Z. J. Shen, “1 MHz cascaded Zsource inverters for scalable grid-interactive photovoltaic (PV) applications using GaN device,” in Proc. IEEE Energy Convers. Congr. Expo., Sep. 17-22, 2011, pp. 2738–2745.

[7] B. Ge, Q. Lei, F. Z. Peng, D. Song, Y. Liu, and A.R. Haitham, “An effective PV power generation control system using quasi-Z source inverter with battery,” in Proc. IEEE Energy Convers. Congr. Expo., Sept. 17-22, 2011, pp.1044-1050.

[8] Y. Zhou, L. Liu, and H. Li, “A high-performance photovoltaic moduleintegrated converter (MIC) based on cascaded quasi-Z-source inverters (QZSI) using eGaN FETs,” IEEE Trans. Power Electron., vol. 28, no. 6, pp. 2727–2738, Jun. 2013.

[9] Y. Zhou and H. Li, "Analysis and Suppression of Leakage Current in Cascaded-Multilevel-Inverter-Based PV Systems," IEEE Trans. Power Electron., vol.29, no.10, pp.5265-5277, Oct. 2014.

[10] L. Liu, H. Li, Y. Xue and W. Liu, “Decoupled Active and Reactive Power Control for Large-Scale

ISSN 2394-3777 (Print)
ISSN 2394-3785 (Online)
Available online at www.ijartet.com
International Journal of Advanced Research Trends in Engineering and Technology (IJARTET)
Vol. 4, Issue 4, April 2017

Grid-Connected Photovoltaic Systems Using Cascaded Modular Multilevel Converters," IEEE Trans. Power Electron., vol.30, no.1, pp.176-187, Jan. 2015.
[11] D. Sun, B. Ge, F. Z. Peng, A. R. Haitham, D. Bi, and Y. Liu, "A new grid-connected PV system based on cascaded H-bridge quasi-Z source inverter," in Proc. IEEE Int. Symp. Ind. Electron., May 28–31, 2012, pp. 951–956.
[12] Y. Liu, B. Ge, A. R. Haitham, and F. Z. Peng, "A modular multilevel space vector modulation for photovoltaic quasi-Z-source cascade multilevel inverter," in Proc. IEEE App. Power Electron. Conf., Mar. 17–21, 2013, pp. 714–718.
[13] F. Guo, L. Fu, C. Lin, C. Li, W. Choi and J. Wang, "Development of an 85-kW Bidirectional Quasi-Z-Source Inverter With DC-Link FeedForward Compensation for Electric Vehicle Applications," IEEE Trans. Power Electron., vol.28, no.12, pp.5477,5488, Dec. 2013. [14] T. P. Parker "Reliability in PV inverter design: black art or sciencebased discipline?" Solarbridge Technologies white paper.